PCCP

ROYAL SOCIETY OF CHEMISTRY

PAPER

View Article Online
View Journal | View Issue

Cite this: *Phys. Chem. Chem. Phys.*, 2025, **27**, 9573

Enhanced oil recovery promoted by aqueous deep eutectic solvents on silica and calcite surfaces: a molecular dynamics study†

Alok Kumar,[a] Swasti Medha,[a] Devargya Chakraborty,[a] Debashis Kundu[b] and Sandip Khan *[a]

Enhanced oil recovery (EOR) plays a critical role in optimizing oil extraction from existing fields to satisfy global energy demands while mitigating environmental impact. One promising EOR technique involves injecting water with reduced surface tension utilizing deep eutectic solvents (DESs). Despite early experimental support, the efficacy of aqueous–DES EOR varies and depends on factors such as connate water saturation, water salinity, and reservoir wettability. The recovery mechanisms for aqueous DESs are poorly understood due to the intricate nature of oil components and reservoir formation. In this paper, we investigate the role of DESs in the EOR process through molecular dynamics (MD) simulations. Three different types of DES molecules, such as choline chloride : urea (ChCl : U), choline chloride : ethylene glycol (ChCl : EG), and menthol : salicylic acid (M : SA) are used, for the recovery of dodecane ($C_{12}H_{26}$) oil from silica and calcite confined surfaces. We have demonstrated the structural characteristics of these systems by examining various physical properties, including interaction energies, density profiles, hydrogen bonds, and interfacial tension (IFT). Different concentrations (10 and 25 wt%) of DESs have been considered to unravel the effect of concentration on oil removal. The wettability of the substrate and the IFT between oil and aqueous DESs are critical physical properties that play a crucial role in influencing EOR phenomena. The IFT between water and oil decreases with the addition of DESs for all DES molecules, leading to a shift in surface behavior from oleophilic to oleophobic and ultimately facilitating the removal of oil from the substrate. Additionally, hydrogen bond formation between DESs and water has been calculated to elucidate its influence on the water/oil interface and substrate wettability. The study provides insights into the fundamental aspects of EOR processes for more effective and sustainable oil extraction.

Received 29th December 2024,
Accepted 25th March 2025

DOI: 10.1039/d4cp04888a

rsc.li/pccp

1. Introduction

Conventional oil recovery methods are inadequate for extracting the remaining heavy crude oil from reservoirs worldwide.[1] However, enhanced oil recovery (EOR) methods present a promising solution for recovering much of this oil.[2] Numerous economic and technological factors influence the selection of the method and the anticipated recovery. According to the U.S. Department of Energy, only one-third of the total available oil is currently produced globally.[3] Utilizing EOR methods facilitates increased oil production in response to the growing demand.[3] The widely recognized conventional chemical EOR methods include polymer flooding, surfactant flooding, and alkaline flooding.[4] In chemical EOR, the key mechanisms involved are wettability alteration, interfacial tension (IFT) reduction, and viscosity improvement.[5]

Nevertheless, traditional chemical methods for EOR face certain restrictions.[6,7] For example, polymer flooding, which primarily enhances recovery by augmenting injection viscosity and, subsequently mobility, encounters viscosity reduction in the presence of reservoir brines and elevated temperatures.[2,8] Similarly, surfactants and alkalis experience diminished efficacy as they flow through porous media due to adsorption phenomena.[9,10] Consequently, diverse alternative chemical flood injection approaches have been implemented for EOR processes.[10] In recent years, novel solvents such as ionic liquids (ILs) and deep eutectic solvents (DES) have emerged as recovery agents, attracting significant research attention due to their tailored design to match the distinctive features of specific reservoirs.[11–15]

[a] *Department of Chemical and Biochemical Engineering, Indian Institute of Technology Patna, Patna, 801106, India. E-mail: skhan@iitp.ac.in*
[b] *Department of Chemical Engineering, Institute of Chemical Technology Marathwada Campus, Jalna, Maharashtra 431203, India*

† Electronic supplementary information (ESI) available. See DOI: https://doi.org/10.1039/d4cp04888a

In recent years, there has been a growing trend in studying the EOR process using both theoretical and experimental approaches, with a particular emphasis on MD simulations.[16–18] The critical aspect of MD research related to EOR is studying oil/water interfacial properties involving surfactants, polymers, foams, and nanoparticles as EOR agents at the molecular level.[19] So far, MD simulations have been instrumental in enhancing various EOR methods, including chemical EOR,[5,20,21] CO_2-EOR,[22–24] and thermal EOR.[25] These simulations help evaluate the effectiveness of new EOR agents, predict gas characteristics, and analyze fluid behaviors. By modeling molecular interactions at the oil/water interface, MD simulations can forecast aggregation patterns and identify optimal conditions for experimental setups. This capability bridges theoretical research with practical application, guiding the development of innovative oil recovery agents.[19,22–24,26]

Understanding the performance of oil displacement agents on the rock/ore surface using MD simulations requires considering wettability as a crucial factor. Wetting, or wettability, describes how effectively a liquid interacts with and spreads across a solid surface.[27–29] It is a fundamental property of porous surfaces and holds significant importance in the realm of EOR. It can be characterized in terms of oleophilic/hydrophilic and oleophobic/hydrophobic properties, which are determined by the contact angle formed by the liquid of interest on the surface. This measurement is further utilized in various computational methods for illustration.[30] The dynamics of surface wettability extend beyond intrinsic properties, evolving through deliberate modification *via* additives (organic and inorganic) and thermal modifications.[31–33] For example, Manshad and co-authors conducted a study on the impact of wettability alterations and IFT using additives such as ILs.[34] Additionally, they proposed that surfactant flooding can potentially recover oil from carbonate rock-based reservoirs by reducing IFT and modifying wettability.[34] Furthermore, many researchers have studied the wetting behavior of various substances on different surfaces using MD simulations. In this regard, Bhattacharjee *et al.*[35] investigated the wetting performance of aqueous ILs and monitored the spreading of IL molecules across the droplet. Additionally, they highlighted the crucial role of hydrogen bond formation in determining wettability.

ILs present a viable alternative to conventional surfactants in EOR, offering enhanced capabilities for extracting trapped oil. This is achieved by modifying the wettability of reservoir rock from oleophilic to hydrophilic (*i.e.*, oil-wet to water-wet) and concurrently reducing the interfacial tension between oil and water.[36,37] The ability to selectively choose cations and anions enables the creation of task-specific compounds, allowing for the design of ILs tailored to the unique characteristics of individual reservoirs.[38,39] Bera *et al.*[40] conducted a comprehensive review providing an overview of the application of ILs in the field of EOR. They highlighted the tunability and exceptional stability of ILs under harsh reservoir conditions, positioning them as superior alternatives to conventional EOR methods. Furthermore, Buuren *et al.*[41] performed MD simulations to investigate how surface characteristics respond to van der Waals (VdW) parameters at the decane/water boundary. Their observations revealed distinct behaviors of water and decane (oil) molecules at the interface compared to the bulk. Similarly, Kunieda *et al.*[42,43] employed MD simulations to examine the spreading of multicomponent oils on water surfaces, including decane, toluene, and heptane. Their study aimed to elucidate the IFT between the components of water and oil mixtures. Likewise, Zhao *et al.*[44] used MD studies to investigate the impact of salinity on the oil/water interface. Their findings suggested that low-salinity water flooding in rock cores could be a promising method for EOR. Likewise, Sivabalan *et al.*[45] conducted experiments focusing on imidazolium-based ILs. Their findings suggest that wettability alteration significantly impacts EOR processes. The study examined parameters including aging time, IL concentrations, and rock permeability to gain insights into EOR mechanisms. Despite the numerous features of ILs for EOR, they encounter several major challenges.[46] Their synthesis is complex, and some ILs are hazardous. Additionally, high operational costs represent another obstacle.[46]

In contrast to ILs, DESs are also known as a novel and potentially more attractive class of EOR agents. These simple and cost-effective solvents boast higher biodegradability and lower toxicity than their IL counterparts while exhibiting comparable efficiency.[47–49] DESs are composed of a blend of HBDs and HBAs, and at a specific eutectic composition, they exhibit a substantial reduction in melting temperature compared to the individual components of the DESs.[47] Atilhan and co-authors explored the potential of DESs for EOR using MD simulations.[50,51] They observed significant alterations in hydrogen bonding at the aqueous–oil interfaces compared to bulk liquid phases. Furthermore, the presence of DES at low concentrations in water solutions in contact with oil droplets confirmed their efficacy for EOR applications. Recently, Hebbar *et al.* conducted a comprehensive investigation, combining MD simulations and experimental studies, to analyze the aggregation of asphaltene and subsequent separation in the presence of a DES.[52] Similarly, Hadj-Kali *et al.*[53] investigated the influence of incorporating two DESs, namely ChCl : U and ChCl : EG, on the IFT of crude oil/brine systems at varying concentrations and temperatures. Their investigation demonstrated a significant reduction in IFT upon introducing both ChCl : U and ChCl : EG. They found that increasing the temperature and concentration of the DES led to further decreases in IFT. Furthermore, El-hoshoudy and co-authors[54] have conducted both experimental and theoretical investigations utilizing four quaternary ammonium-based DES solutions. The study examined how the rheological properties and interfacial tension-reducing effects of the four DESs interacted with the reservoir conditions. Their study focused on the physicochemical properties and interfacial tension alteration capacity of these DESs.

Despite prior research on EOR, the focus has predominantly been on classical DESs, often neglecting the intricate and varied surface structures. Additionally, there remains a significant gap in research regarding the systematic and comprehensive understanding of the wetting transition

mechanisms of DESs in oil/water systems on various solid surfaces. Collective research highlights that MD simulations are a powerful tool for uncovering fundamental insights into the structural and physicochemical properties of a system, particularly those that are difficult to measure experimentally. Due to the aforementioned reasons, in our study, we have used three different DESs (ChCl : U, ChCl : EG, and M : SA) with water on two different confined surfaces (silica and calcite). The selection of DESs is based on a thorough screening process using COSMO-RS as shown in our previous publication.[55] In that work, we observed that these specific combinations of HBA:HBD are capable of achieving more than 75% reduction in the IFT due to their hydrophobicity. Therefore, we choose the DES system of menthol and salicylic acid and compared it with the commonly used choline chloride based DESs. To understand the effect of concentration on removing oil molecules from the considered surfaces, we have taken two different compositions: 10 wt% and 25 wt% DES in water. Here, we observed that, among various analyses such as density profile and hydrogen bond analyses, the menthol based DESs have enhanced oil recovery capabilities compared to traditional choline-chloride based DESs. These findings were further confirmed by the density contours, which revealed the formation of sizable, localized oil aggregates on calcite and silica surfaces when a DES was present. Subsequent examinations of interfacial tension further supported these observations, demonstrating a reduction across all DES systems when oil was added. Notably, M : SA displayed the most significant decline in interfacial tension. These collective results emphasize the potential utility of DES formulations in advanced EOR strategies.

2. Model and methodology

2.1. Aqueous–DES–oil model

In this section, MD simulations were conducted on three DESs: ChCl : U, ChCl : EG, and M : SA. These DES systems were combined as depicted in Fig. 1. The compositions involved the mixture of U and EG with ChCl molecules in a fixed ratio of 1 : 2, and similarly for menthol–salicylic acid in a ratio of 4 : 1. For packing purposes, the PACKMOL[56] tool was employed. Subsequently, the prepared DES systems introduced 6000 water molecules and 200 oil molecules (dodecane, $C_{12}H_{26}$). The choice of the SPC/E water model[57,58] was based on its computational efficiency with reasonable accuracy for initializing the liquid configuration. Due to the complexity of modelling crude oil, molecular simulations often use dodecane as an oil medium for the study of enhanced oil recovery.[59–62] Dodecane is a major component of gasoline, diesel, and kerosene, making it a suitable model for lighter crude oil fractions. The number of DES molecules required was calculated based on the presence of 6000 SPC/E water molecules for concentrations of 10% and 25%, as summarized in Table 1.

2.2. Surface modelling

2.2.1. Silica. The SiO_2 slab was modeled using the INORGANIC-builder tool of VMD.[63] A silica surface with dimensions of 9.956 × 6.250 × ∼1 nm^3 was employed to prepare the

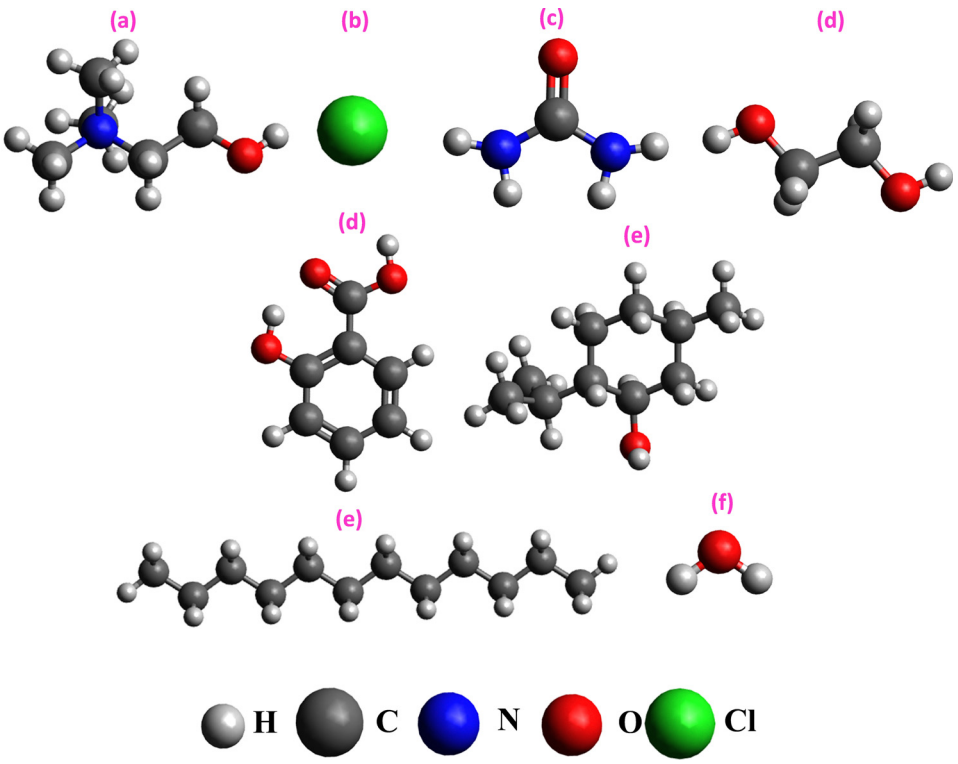

Fig. 1 All-atom representation of (a) choline $(Ch)^{(+)}$, (b) chloride $(Cl)^{(-)}$, (c) urea (U), (d) ethylene glycol (EG), (e) salicylic acid (SA), (f) menthol (M), (g) dodecane (Oil), and (h) water.

Table 1 Number of DES molecules corresponding to 6000 water molecules

wt% of DES	ChCl : U (1 : 2)	ChCl : EG (1 : 2)	M : SA (4 : 1)
10	46 : 92	46 : 92	60 : 15
25	138 : 276	137 : 274	188 : 47

confined system as illustrated in Fig. 2b. The periodic boundary conditions (PBC) were applied in all directions. However, in the vertical (y) direction, a vacuum space of 20 nm was maintained including the confined system to prevent interactions with periodic images of molecules.

2.2.2. Calcite. In the case of the $CaCO_3$ system, unit cell data from the work of Xiao *et al.*[64] were utilized and generated using VMD to create a surface measuring 9.976 × 6.800 × ~1 nm^3 as shown in Fig. 2(c). The confinement of the system was accomplished similarly to the silica surface using the same PBC that was used in the case of the silica surface.

2.3. Computational modeling of the confined system

To explore how three DES molecules interact with different surfaces, *i.e.*, SiO_2 and $CaCO_3$, molecular dynamics (MD) simulations were conducted using GROMACS (version – 2018.2) software.[65] The OPLS/AA force field[66] was employed to model the intermolecular and intramolecular interactions for choline-based DESs. This force field reproduces the physical properties of DESs, such as density, surface tension, and viscosity, in good agreement with experimental values. For menthol-based DESs, the force field was modeled using LIGPARGEN[67–69] (see Table S1, ESI†). Throughout the simulations, all surfaces were maintained as rigid. The SiO_2 force field was adapted from the work of Cruzchu *et al.*,[70] and the $CaCO_3$ model and force field were based on Xiao *et al.*'s[64] research. Interaction parameters between DES molecules and surfaces were calculated using the Lorentz–Berthelot mixing rule.[71] Energy minimization was achieved using the steepest-descent algorithm to ensure a stable configuration. An annealing run for 2 ns at a temperature of 500 K was conducted to rearrange the molecules and make the systems devoid of any metastable state. During the annealing run, the temperature was maintained at 298, 500, and 298 K for 0, 150, and 2000 ps. Subsequently, a 100 ns canonical ensemble (NVT) simulation was performed with a time step of 1 fs, also applying a 1.2 nm cut-off for coulombic and van der Waals interactions. A Noose–Hoover thermostat was applied during the simulation to keep the temperature of the system constant at 298 K. Long-range electrostatic interactions were calculated using the particle mesh Ewald[72] (PME) method. The final configuration files were visualized and examined using the VMD software package.[63]

We simulate a confined oil ($C_{12}H_{26}$) molecule system in the presence of aqueous–DES molecules to explore the oil interactions with the silica and calcite surfaces. The preliminary configurations for the simulation models are illustrated in Fig. 2a. We have taken the oil layer near the sheet (100 molecules at the bottom and 100 molecules at the top sheet) and water–DES between the oil layer (Fig. 2a). In addition, to understand whether DESs play any major role, we prepared two systems with only oil and water molecules on SiO_2 and $CaCO_3$ surfaces. Therefore, we have 6 systems each for silica and calcite surfaces including 3 different DES systems of various concentrations and 2 systems having an exactly similar configuration with no DES molecules.

3. Results and discussion

3.1. Solid–fluid interaction energy

The equilibration of the confined aqueous DES and oil systems is confirmed by plotting the total interaction energy (coulombic + LJ) of all the species concerning the substrates. In the case of the

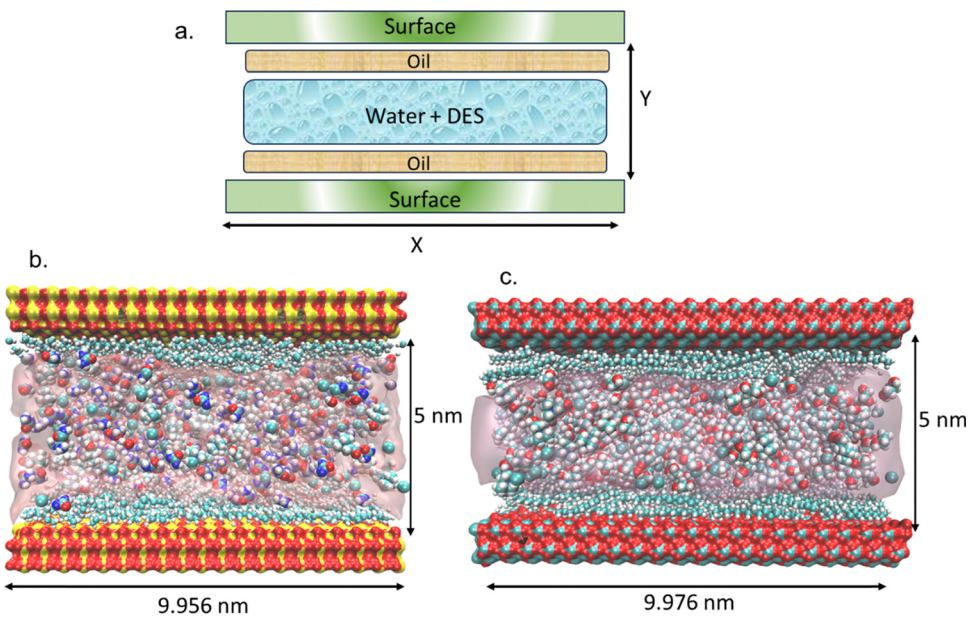

Fig. 2 The initial configuration of the confined water–DES/oil system: (a) schematic of the initial configuration, (b) SiO_2 surface, and (c) $CaCO_3$ surface.

calcite surface, we observed that the coulombic interactions are much more dominant compared to VdW (LJ) interactions (see Fig. 3(d–f)). On the silica (SiO_2) surface, the magnitude of total interaction energy is much less than that in the case of the $CaCO_3$ surface due to the higher coulombic energy associated with the calcite surface. We initially observed ($t < 10$ ns) that the oil molecules interact much more with the surface, which may be due to the initial geometry of the system (see Fig. 2(a)), but with the evolution of time, the water interaction energy starts to decrease ($t < 40$ ns) more and finally the interaction of oil gets displaced by water molecules. After $t > 85$ ns, the energy becomes almost constant for all the DES systems (see Fig. 3(a–c)).

In the case of both surfaces, the DES molecules equilibrate much faster than oil and water molecules. The interaction energy gives a picture of the favorable interactions of molecules with the substrates but does not give a complete insight into the preferential adsorption of specific molecules near the surface and how it changes with the addition of different DES systems at different concentrations. To understand this, we studied the density distribution of all the involved molecules (oil, water, and DES) in the next section.

3.2. Wetting performance of oil in the presence of an aqueous DES in a confined system

To characterize the wetting behavior of oil in the presence of an aqueous DES sandwiched between the surface (as shown in Fig. 2a), we analyze the density profile along the vertical axis relative to the surface. Density profiles and contours are computed using the equilibrated systems from the final 5 ns of the simulations.

3.2.1. Silica (SiO_2) surface. We perform the oil–water simulation in the absence of DES molecules to observe the behavior of oil in the presence of only water. Oil is introduced into a confined aqueous medium on a silica surface (see Fig. S1 in the ESI† document). We observe that oil molecules aggregate in the bulk (see Fig. 4), but a strong layering of oil is found near the silica surface. This is indicated by the spike in density values near the surface and the deep red color in the contour (Fig. 4a and b, respectively). To investigate the removal of oil from the silica surface, we introduced three different DES molecules (ChCl : EG, ChCl : U, and M : SA) at varying concentrations
(10 wt% and 25 wt%) and observed the resulting phenomena.

Now, we added 10 wt% DES molecules to an oil–water system (see Fig. 2) and equilibrated it for 100 ns, as demonstrated in Fig. 3. The density plots of the water–DES and oil system on the SiO_2 surface are shown in Fig. 5. We observe that, with the partial replacement of oil by a DES, the density spike of the oil near the sheet disappears, indicating that the oil molecules are moving toward the bulk of the system. This occurs because the DES molecules form an interface layer between the oil and the sheet, a phenomenon observed consistently across all three DES molecules studied. Additionally, DES molecules form an interface between water and oil, decreasing the IFT of oil and water. Further increasing the DES wt% enhances the oil displacement and eventually leads to its complete detachment from the surface, as shown in Fig. 5(d–f) for 25 wt%.

The validity of the aforementioned finding can be confirmed by examining the density contours of the systems, as illustrated in Fig. 6–8 (for ChCl : U, ChCl : EG, and M : SA, respectively). The contours distinctly reveal oil displacement from the surface in the presence of an aqueous DES for 25 wt% DES systems. This effect is particularly pronounced in ChCl : U and M : SA compared to ChCl : EG. The distribution of DES molecules in the bulk, as evidenced by the density profile, underscores their proximity to oil molecules, a relationship visualized in the density contour.

The oil molecules, as observed from the density profile (see Fig. 5), are surrounded by the urea molecules and are present in the bulk of the system (see Fig. 6(d)). The EG molecules, unlike urea molecules, are present throughout the system and more

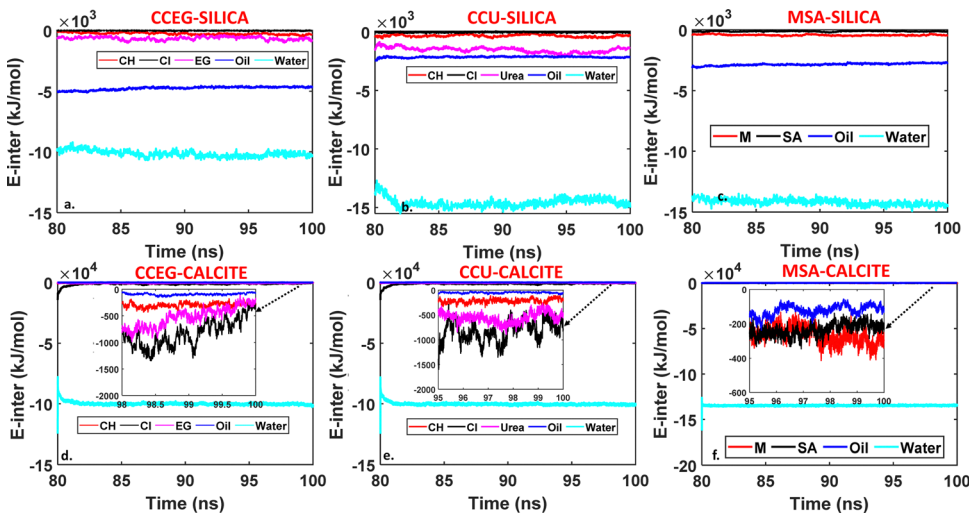

Fig. 3 Interaction energy of 10 wt% ChCl : U based DES on SiO_2 and $CaCO_3$: (a)–(c) the total (coulombic and LJ) interaction of different components with SiO_2 and (d)–(f) the total (coulombic and LJ) interaction with $CaCO_3$ (the values in the inset represents the final values of the interaction energy).

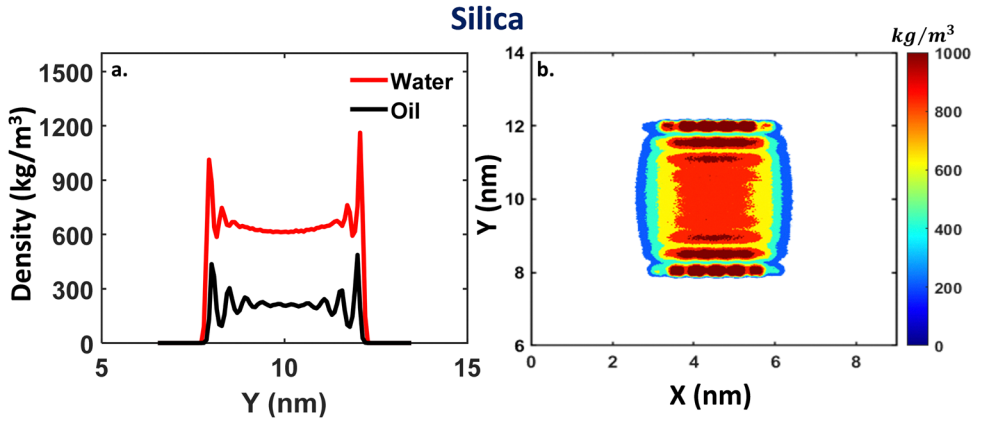

Fig. 4 (a) Density profile of oil and water in the absence of DES molecules on a confined SiO_2 surface. (b) 2D density contour of oil molecules on a confined SiO_2 surface in the absence of any DES molecules.

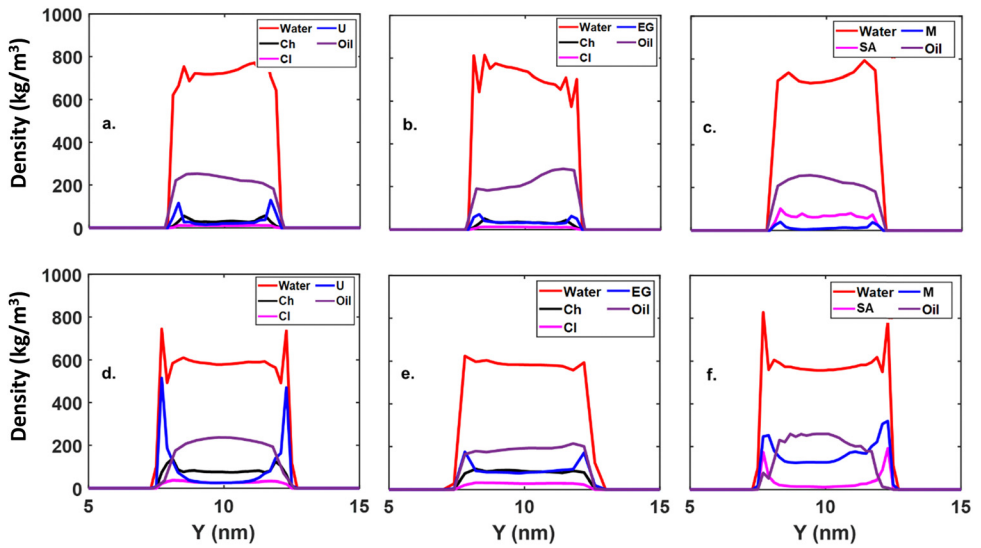

Fig. 5 Density outline along the *Y*-axis of the water–DES/oil system on the SiO_2 surface: (a)–(c) 10 wt% of water–DES/oil system for ChCl : U, ChCl : EG, and M : SA, respectively; (d)–(f) 25 wt% of water–DES/oil system for ChCl : U, ChCl : EG, and M : SA, respectively (the *Y*-axis is perpendicular to the surface).

densely at the solid–liquid interface and the liquid–liquid interface (water–oil) (Fig. 7(b)). Lastly, when M : SA is introduced into the system, we observed similar results to the ChCl : U system, *i.e.*, the oil molecules were surrounded by DES molecules.

Furthermore, in the ChCl : U system, urea (HBD) shows exceptional oil removal capabilities and concentrates near the sheet, as evidenced by the density contour in Fig. 6b. Conversely, in the M : SA system, menthol (HBA) encircles the oil droplet (oleophilic in nature), suggesting its effectiveness in oil removal (Fig. 8d), significantly reducing IFT due to its presence at the water–oil interface. As a result, the M : SA system is likely more potent for oil removal applications due to the lower IFT. In a later section, we will quantify the IFT values for the three systems to support this observation.

3.2.2. Calcite ($CaCO_3$) surface. In contrast to Fig. 4, which depicts a strong oil layer adsorbed on silica, oil molecules introduced to calcite become surrounded by water molecules, as visualized in the density contour in Fig. 9. This observation is further supported by the density profile in Fig. 9a, which lacks any evidence of oil layering closer to the calcite surface. This phenomenon could be attributed to the strong coulombic interactions between water molecules and the calcite surface, as illustrated in Fig. 3d–f. Furthermore, to elucidate the influence of various DES molecules on the oil–water system in the presence of calcite, three DES variants (ChCl : U, ChCl : EG, and M : SA) were introduced at different concentrations.

Analysis of the density profiles in Fig. 10a–f for 10% and 25% DES concentrations reveals intriguing insights into the interplay between oil, water, and DES at the calcite surface. Consistently across all systems, water molecules exhibit a strong affinity for the surface, evidenced by their presence near the calcite sheet and throughout the bulk (Fig. 10). This observation reinforces the previously established strong interaction between water and the calcite surface.

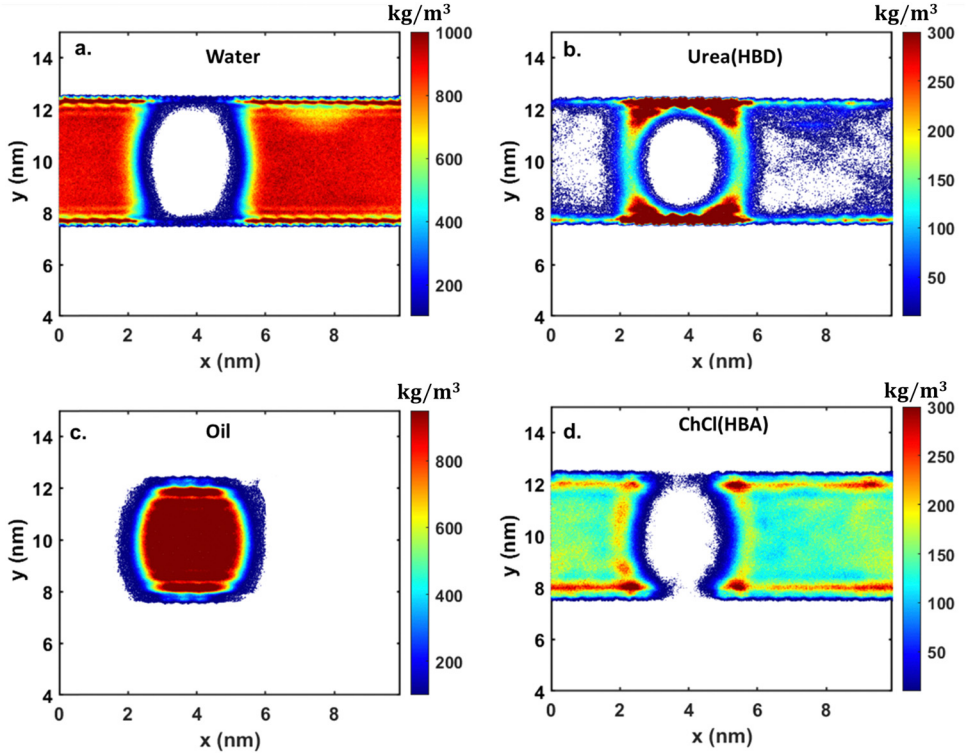

Fig. 6 2D density contour under confinement for a 25 wt% system of ChCl : U on SiO_2, depicting the distribution of (a) water, (b) urea, (c) oil, and (d) ChCl.

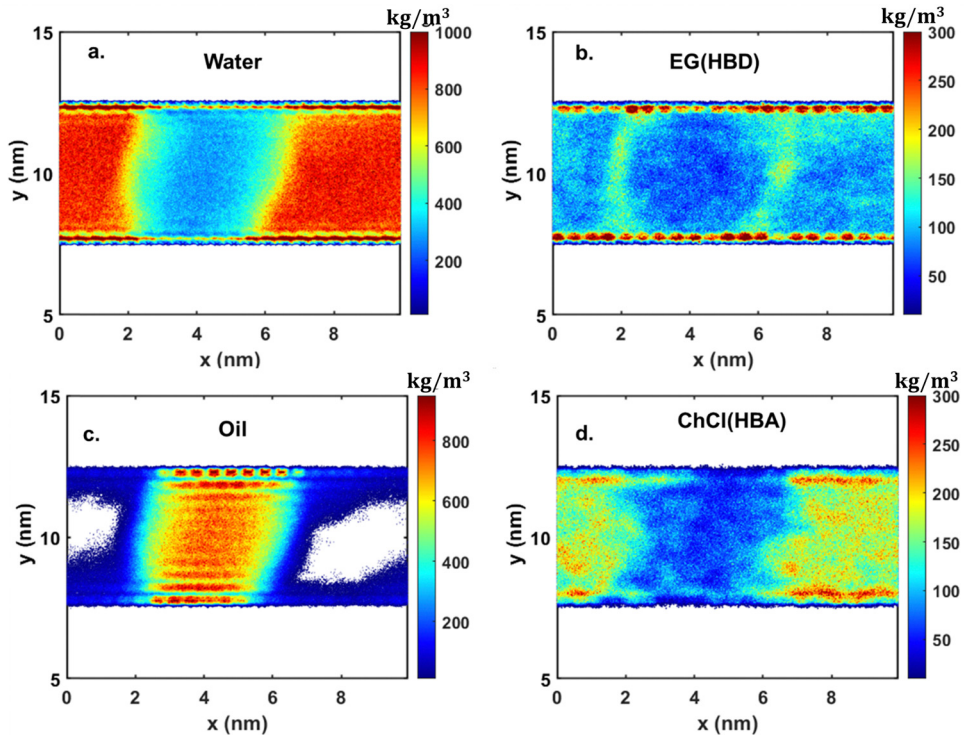

Fig. 7 2D density contour under confinement for a 25 wt% system of ChCl : EG on SiO_2, depicting the distribution of (a) water, (b) EG, (c) oil, and (d) ChCl.

The introduction of DES molecules primarily affects the bulk phase. As the concentration of HBD species in the DES increases (from 10 wt% to 25 wt%), the corresponding peak in the density profile intensifies, as shown in Fig. 10. This suggests a preferential distribution of DES molecules within the bulk solution. Finally, the density profiles offer compelling evidence

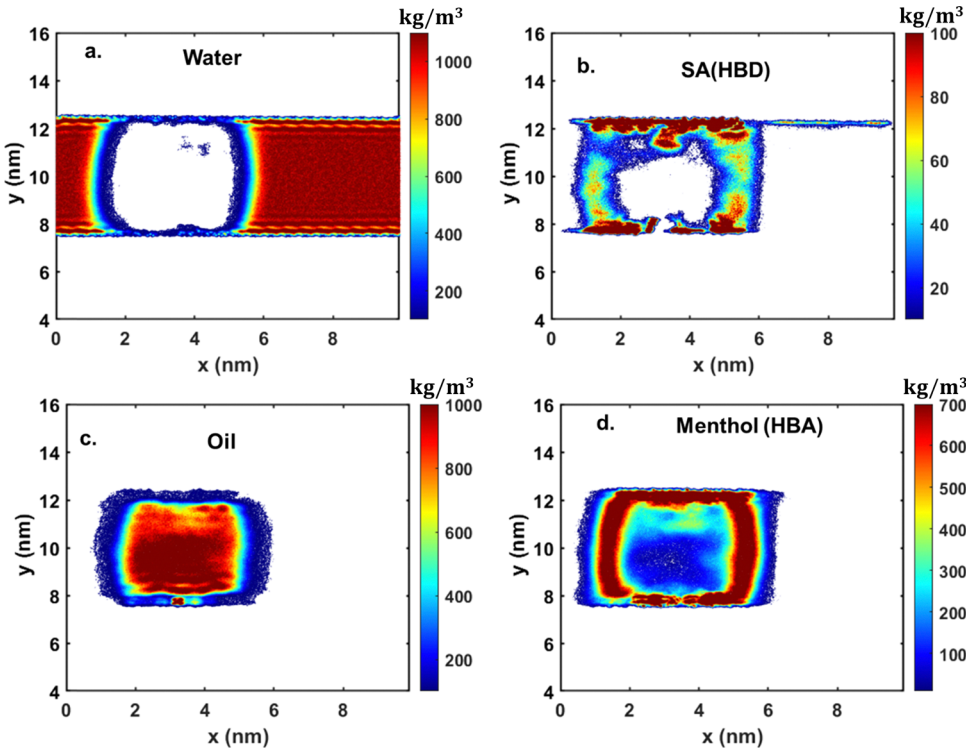

Fig. 8 2D density contour under confinement for a 25 wt% system of M : SA on SiO_2, depicting the distribution of (a) water, (b) SA, (c) oil, and (d) menthol.

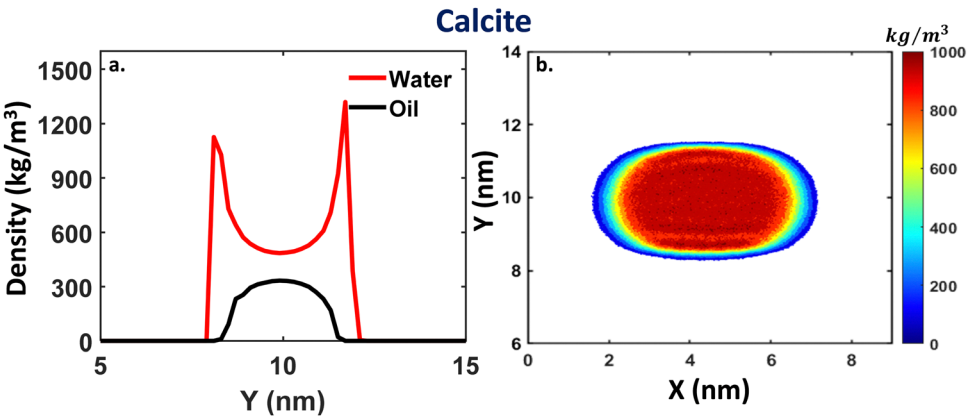

Fig. 9 (a) Density profile of oil and water without any DES molecules on a confined $CaCO_3$ surface. (b) 2D density contour of oil molecules on a confined $CaCO_3$ surface without any DES molecules.

for oil removal from the calcite surface. The absence of a distinct oil peak near the surface at both DES concentrations (Fig. 10) indicates a shift in oil distribution towards the bulk phase.

Similar to the findings on SiO_2, the above results for 25% DES on the $CaCO_3$ surface can also be verified through the density contour profile of individual components. In the case of the $CaCO_3$ surface, when ChCl : U is added, the results were very similar to those on the silica surface. The urea molecules showed preferential aggregation near the oil interface (see Fig. 11), whereas ChCl molecules are present throughout the system (see Fig. 11d). As shown in Fig. 11c, the oil molecules form a cluster, but unlike the silica surface, the shape is much more spherical, ensuring no layer formation with the surface.

In contrast to the silica surface, where the oil molecules were getting attracted towards the surface and, as a result, an oil–DES droplet formation occurred, no such phenomenon was observed on the calcite surface. The oil molecules are found to interact with the ChCl : EG molecules, mimicking the behavior of the ChCl : U system on the calcite surface. The density contour shows that the oil molecules show similar spherical aggregation (see Fig. 12). The only difference observed is in the

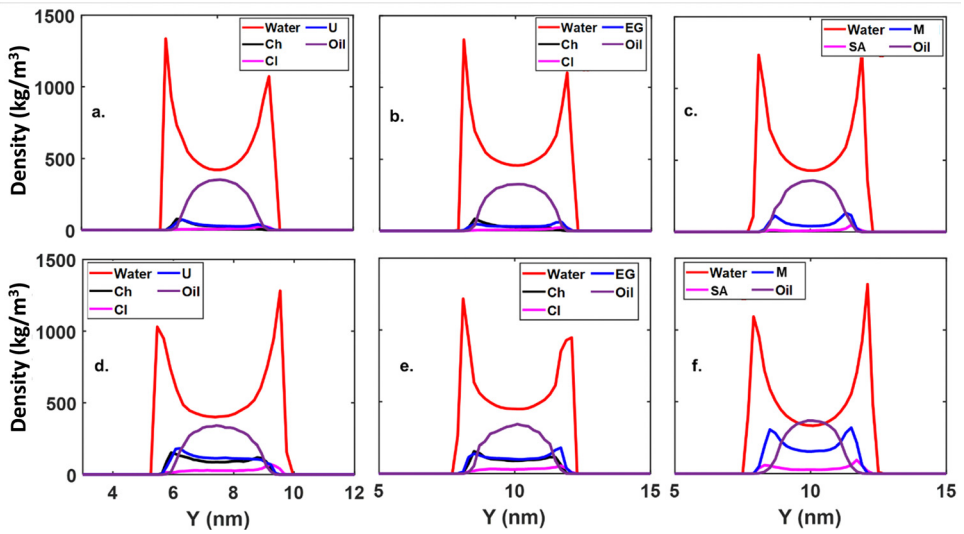

Fig. 10 Density outline along the *Y*-axis (normal to the surface) for the water–DES/oil system on the $CaCO_3$ surface: (a)–(c) 10 wt% of water–DES/oil system for ChCl : U, ChCl : EG, and M : SA, respectively, and (d)–(f) 25 wt% of water–DES/oil system for ChCl : U, ChCl : EG, and M : SA, respectively.

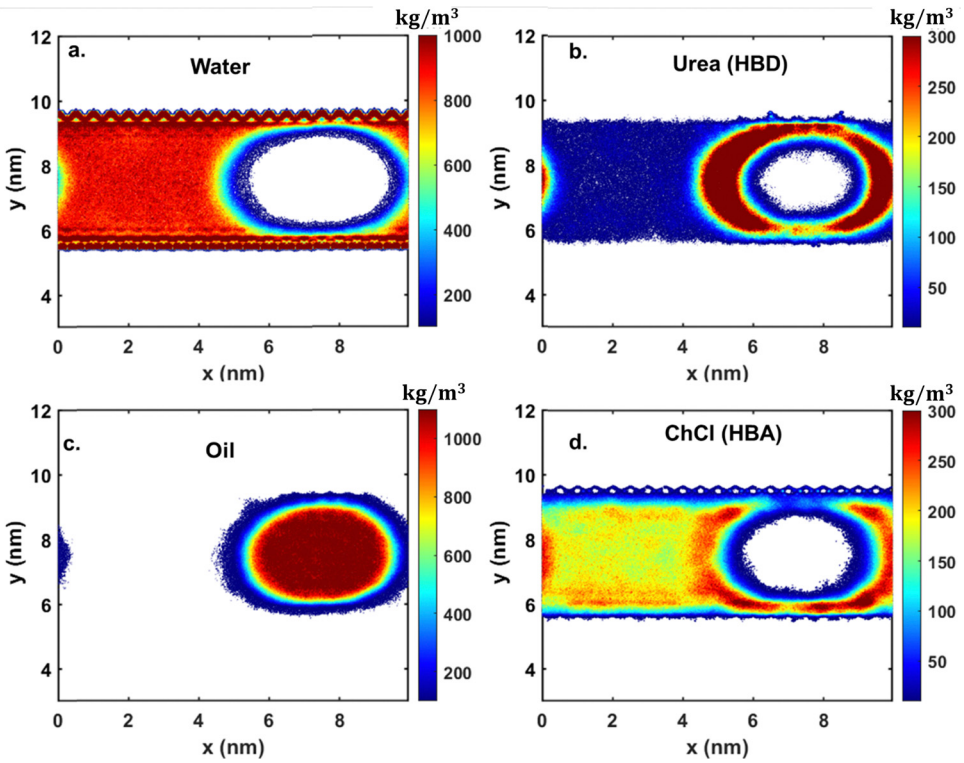

Fig. 11 2D density contour under confinement for a 25 wt% ChCl : U system on a $CaCO_3$ surface, depicting the distribution of (a) water, (b) urea, (c) oil, and (d) ChCl.

distribution of DES molecules. Both EG and ChCl molecules are distributed throughout the confined system, with EG molecules being densely placed near the oil–water interface, whereas ChCl shows no such preferential behavior and is distributed throughout the system (see Fig. 12d).

Lastly, M : SA shows contrasting behavior compared to the other two DES systems. The oil molecules, unlike ChCl : U and ChCl : EG systems, where there was an aggregation in the form of a spherical structure (see Fig. 11c and 12c), do not show similar behavior (see Fig. 13); although there is an aggregation of oil molecules, from the density profile, it is clear that much more oil molecules are also dispersed in the system. This behavior could be because SA molecules break at the oil–water interface (see Fig. 13b), resulting in the dispersion of oil

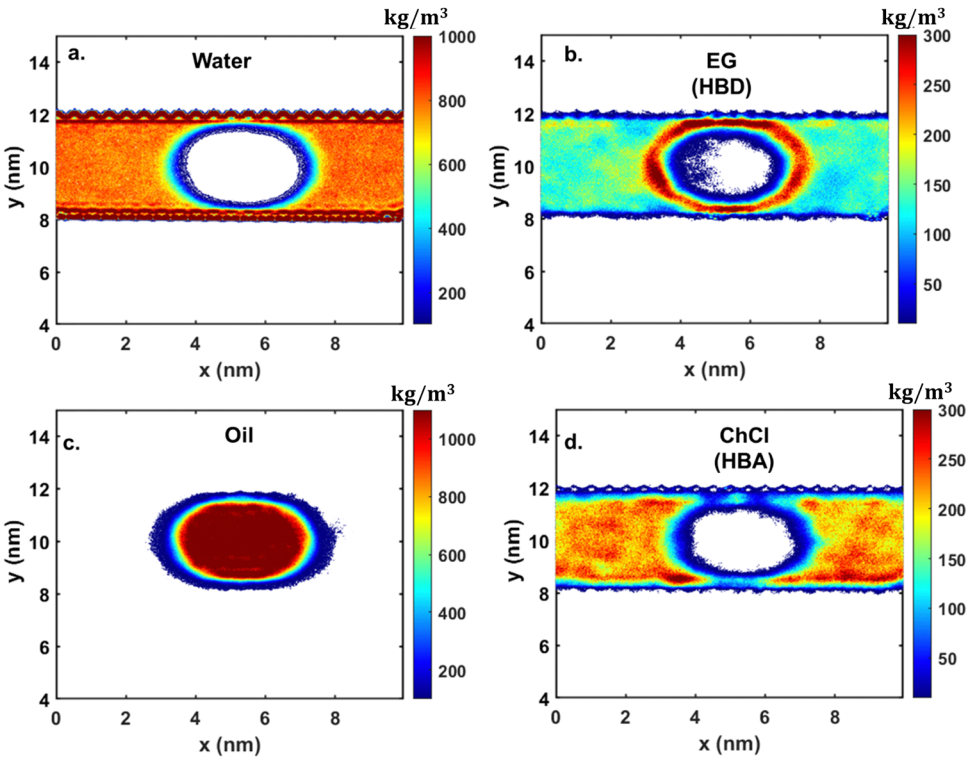

Fig. 12 2D density contour under confinement for a 25 wt% system of ChCl : EG on $CaCO_3$, depicting the distribution of (a) water, (b) EG, (c) oil, and (d) ChCl.

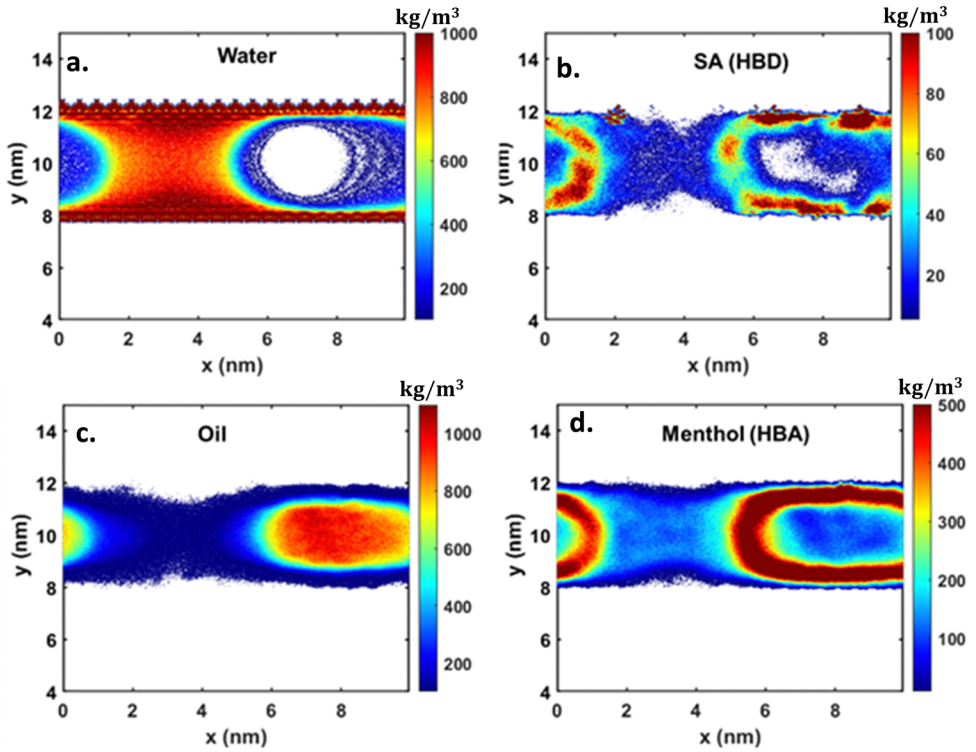

Fig. 13 2D density contour under confinement for a 25 wt% system of M : SA on $CaCO_3$, depicting the distribution of (a) water, (b) SA, (c) oil, and (d) menthol.

molecules throughout the system. However, the menthol molecules show aggregation near the oil–water interface (see Fig. 13d), which could be why some oil molecules form clusters.

3.3. Oil recovery evolution

Fig. 14 and Fig. 15 illustrate the temporal evolution of oil recovery from the SiO_2 and $CaCO_3$ surfaces for the ChCl : U water–oil system. Refer to the ESI† document (see Fig. S2–S5) for the other two systems, ChCl : EG and M : SA. Furthermore, for clarity, only oil molecules are depicted. On the SiO_2 surface, a significant portion of oil molecules initially accumulates near the surface, as shown in Fig. 14. Then, around 12 ns, some oil molecules appear to bridge the gap between the two oil layers. However, in the long run, the aqueous DES displaces all the oil molecules from the surface due to the strong interaction between the urea and water molecules with the SiO_2 sheet, ultimately leading to oil detachment from the sheet.

Conversely, on $CaCO_3$, the dynamics are much faster compared to SiO_2. Around $t \sim 2$ ns, the oil layer starts accumulating, and after 5 ns, the layer detaches from the surface. At around 10 ns, the droplet starts forming, and a complete droplet is formed within a few nanoseconds. This suggests that the calcite surface interacts more with water and, further prompted by the DES, eventually leads to the replacement of the oil layer on the surface.

A side-by-side comparison of the final configuration of the water–DES structure on SiO_2 and $CaCO_3$ is performed (see Fig. S6, ESI†), which shows that, on SiO_2, the DES (ChCl) molecules primarily accumulate near the sheet, whereas on $CaCO_3$, they predominantly gather around the oil rather than near the sheet. Furthermore, the urea molecules at the oil interface might enhance oil interaction, making it more oleophilic than ChCl alone on both surfaces. This observation supports the potential of the water–ChCl : U solution for pulling out oil from solid surfaces.

However, in the case of $CaCO_3$, water seems to be the primary driver of oil recovery compared to urea, as discussed

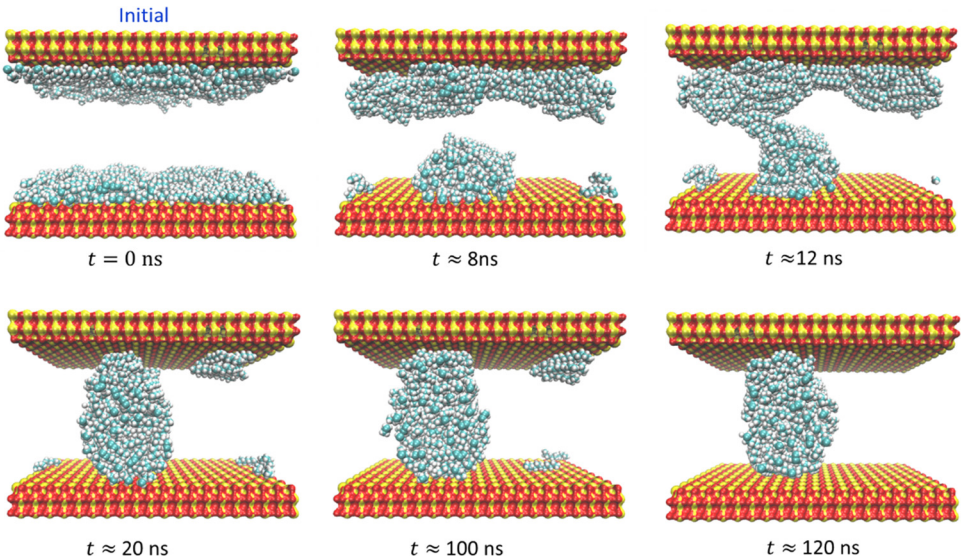

Fig. 14 The evolution of the oil layer on the confinement in the vicinity of water–DES (water–ChCl : U) on the SiO_2 surface.

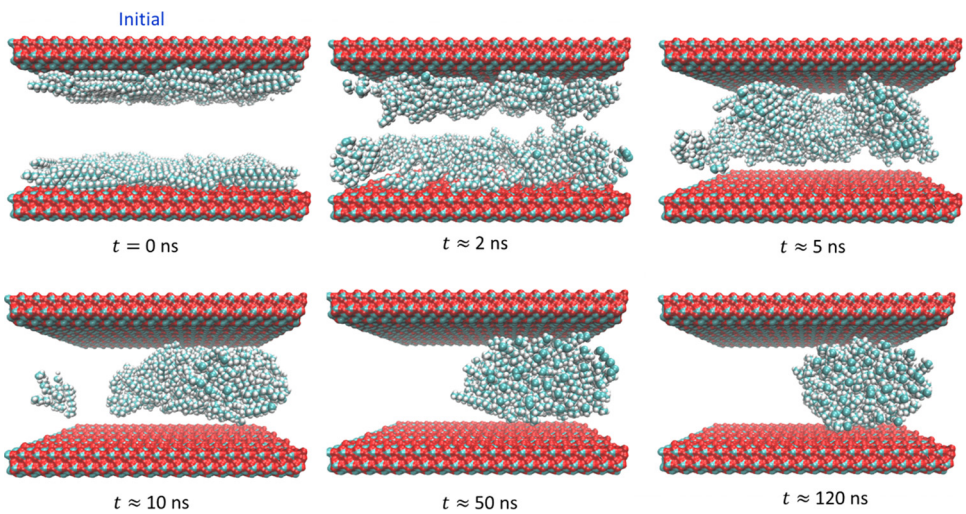

Fig. 15 The evolution of the oil layer on the confinement in the vicinity of water–DES (water–ChCl : U) on the $CaCO_3$ surface.

earlier. Although urea molecules might form a stable layer with oil and water, their role appears less significant than the direct interaction of water with the $CaCO_3$ surface.

So far, we examined the presence of different DES molecules across the system to understand the oil extraction process at the nanoscale. To gain further insights, we will now explore the HB interactions among all the species involved.

3.4. Hydrogen bond analysis

As observed by previous researchers, DES molecules have excellent capabilities of establishing hydrogen bonding (HB) with itself and with polar molecules like water.[73–76] To understand the role of hydrogen bonding in EOR, we calculated the average HB strength of all the components involved using the geometric criteria of Luzar and Chandler[77] (see Fig. S7 and Table S2 in the ESI† document). The HB analysis will give more detailed insights into how oil recovery could take place on different surfaces and how different DESs alter the EOR mechanism. In this work, we calculated the average number of HBs formed and normalized it with the total number of water molecules present in the aqueous–DES system (⟨HB⟩). Since we observed HBs formed with water to be much more dominant compared to DES–DES HBs, we plotted only HBs, which include water–water, HBD–water, and HBA–water, for all three DESs at different concentrations (see Fig. 16).

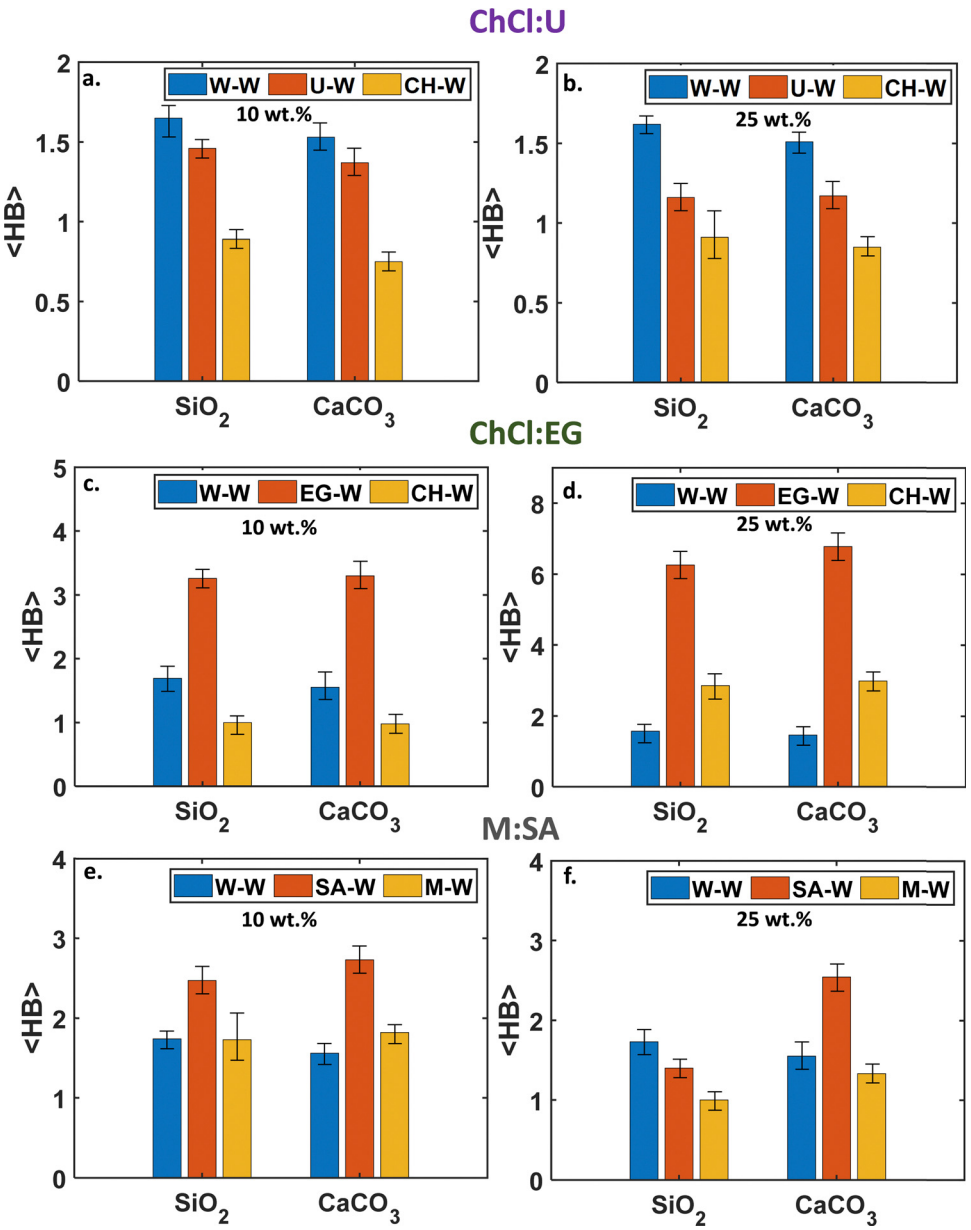

Fig. 16 Average hydrogen bonding (HB) in the DES + water confined system on SiO_2 and $CaCO_3$ (note: all the error bars are calculated using the block average method).

In the case of the ChCl : U system, we observed that, at a lower concentration (10 wt%), the most dominant HB interaction is the water–water HB, which is around ∼1.65 on the silica surface and ∼1.5 on the calcite surface (see Fig. 16(a)). The HB formation of urea–water and choline–water is lower than that of water–water. The HB formation of urea–choline is found to be very small. With the increase in DES concentration (25 wt%) (see Fig. 16(b)), the water–water HB remains the same on both surfaces, but there is a sharp increase in the urea–water HB and choline–water HB, which is expected as the number of acceptor molecules increases in the system. Therefore, HBs in the ChCl : U systems align with the findings from our previous work.[78]

Conversely, for ChCl : EG, it is observed that, at lower concentrations, the EG–water HB is the most dominant one, followed by water–water HB, for both calcite and silica surfaces. The reason could be the structure of the EG molecule, which favors the formation of HB with water. Similarly to ChCl : U, the HB formation between choline and EG (see Fig. 16(c)) is found to be very small. With the increase in the concentration of ChCl : EG, there is only an increase in the average HB strength in the confined system in the order: $HB_{EG-W} > HB_{W-W} > HB_{Cl-W} > HB_{Ch-EG}$ for both calcite and silica surfaces.

In the case of M : SA, we observed that, at a lower DES concentration (10 wt%), SA–water forms the maximum HB, followed by menthol–water (see Fig. 16(e)). As the concentration increases (25 wt%), water–water forms the maximum HB on the silica surface, while no change is observed on the calcite surface. The results show how the formation of HBs in a DES with water changes the dynamics of the whole system, leading to strong layers of DES at the oil–water interface, which eventually leads to the agglomeration of oil molecules.

However, we gained some valuable insights from the density contours and the average HB in the system. There is still a need to understand how the IFT of the aqueous DES is critical in the oil recovery process. To understand this, we discussed the IFT of these aqueous DES systems in the presence of oil.

Table 2 Interfacial tension (IFT) value for oil–water–DES systems

	γ_{LV} (mN m^{-1})		
System	0 wt%	10 wt%	25 wt%
Water/oil	53.50 ± 0.43	—	—
Water–ChCl : U/oil	—	46.80 ± 1.75	48.10 ± 1.25
Water–ChCl : EG/oil	—	46.90 ± 1.20	44.20 ± 1.10
Water–M : SA/oil	—	47.20 ± 1.15	43.05 ± 1.10

3.6. Interfacial surface tension analysis

All three aqueous DES systems with respective wt% are taken and placed inside a cube having dimensions of 6 × 6 × 6 (nm^3). Then, we conducted an NPT simulation of the system at a pressure of 1 bar and a temperature of 298 K for a duration of 10 ns. During the equilibration phase, the volume of the system was observed to stabilize around a specific dimension. After that, the *Z*-direction of the box is extended to three times the original length of the box (L_Z = 3L_X) to perform an NVT simulation for 20 ns. Following this, surface tension was computed by extending the simulation for an additional 20 ns. The surface tension is evaluated using the Irving–Kirkwood method.[79] In this method, the pressure tensor in each direction is calculated individually (P_{XX}, P_{YY} and P_{ZZ}) and then the surface tension (γ_{LV}) is calculated using the equation:

$$\gamma_{LV} = \frac{L_Z}{2} \times \left(\frac{P_{XX} + P_{YY}}{2} - P_{ZZ} \right)$$

where L_Z represents the length of the simulation box in the *Z*-direction, P_{XX} and P_{YY} are the tangential components of the pressure tensor, and P_{ZZ} is the normal component of the pressure tensor.

Initially, during the calculation of the IFT of the oil–water system, we observed its value to be around ∼53 mN m^{-1}. This is considerably less than that of water, which is (using MD simulations) ∼64 mN m^{-1} (ref. 35 and 80) and much more than the surface tension of dodecane, which is around ∼26 mN m^{-1}.[81] This is due to the fact that the oil molecules move towards the vapor–liquid interface, and as a result the favorable interaction between oil–water increases.[82–84] When the aqueous DES solution is mixed with oil and the interfacial tension is calculated, it is observed that, for all the systems, the IFT decreases compared to when the systems are DES-free (see Table 2).

When ChCl : U is applied to the system (10 wt%), the IFT decreases to ∼47 mN m^{-1}. This behavior is due to the presence of urea molecules at the oil–water interface (see Fig. 17(b)), which further disrupts the HB between water–water. As a result, the DES–water interaction increases. When the concentration of DES is increased in the system, interestingly, the IFT value increases to ∼48 mN m^{-1}. Such behavior is also observed in the recent findings of Atilhan *et al.*[51] and also in the experiments conducted by Mohsenzadeh *et al.*[85] for water–DES systems. The authors stated that the increase in the IFT value with the

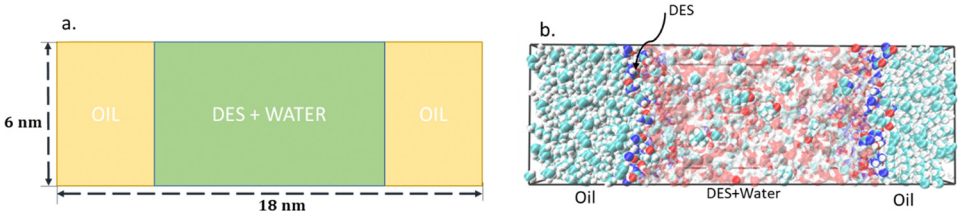

Fig. 17 System setup for the surface tension model: (a) a schematic of the water–DES/oil system and (b) a snapshot of the final equilibrated system for water–ChCl : U/oil at 25 wt%.

increase in DES concentration is primarily due to the reduction in interface thickness, the accumulation and strong interaction of DES molecules at the interface, and the non-linear evolution of interface properties with DES concentration.[85]

Conversely, ChCl : EG and M : SA show a similar behavior, where the IFT value decreases when more DES molecules are introduced into the system.

The IFT study gives a clear picture that the aqueous DES systems can lower the IFT by a reasonable amount, resulting in a better oil recovery process. As the concentration of DES increases in the system, better results are observed in terms of the IFT values (see Table 2).

4. Conclusion

In this study, MD simulations were conducted to examine the potential of aqueous DES systems in enhancing oil recovery processes. Three different DESs, namely ChCl : U, ChCl : EG, and M : SA, were evaluated concerning their interaction with oil molecules (dodecane) on silica and calcite surfaces. Initial assessments of interaction energies and subsequent density profile distributions revealed distinctive behavior among the DES systems. The findings indicate that, compared to systems with no DES molecules on the silica surface, ChCl : U, ChCl : EG and M : SA based silica systems exhibited enhanced oil recovery capabilities by enveloping and effectively recovering oil molecules, and ChCl : U based systems showed a higher drop in the IFT at lower DES concentrations (10 wt%), while M : SA based systems have the best potential for oil recovery at higher DES concentrations (25 wt%) as they show the highest reduction in IFT. On the calcite surface, even without any DES molecules, there is an effective recovery of oil molecules, and this phenomenon is more pronounced when DES molecules (ChCl : U, ChCl : EG, and M : SA) are introduced in the system. From the HB analysis, we observed that HBD–water forms the strongest HBs, and this trend is common in all DESs, which shows that the selection of the HBD plays a pivotal role in this kind of EOR application.

Furthermore, the analysis of interfacial tension highlighted a reduction across all DES systems in the presence of oil, with ChCl : U and M : SA displaying the most significant reduction. These results underscore the promising role of DESs in mitigating interfacial tension, a crucial factor in facilitating oil extraction processes from calcite- and silicate-rich surfaces. The outcomes of this study accentuate the potential utility of DESs in advanced enhanced oil recovery strategies. These findings contribute significantly to understanding the behavior of DESs at oil-rich interfaces, offering prospects for developing innovative methodologies in oil recovery from calcite and silica surfaces.

Abbreviations

EOR	Enhanced oil recovery
DES	Deep eutectic solvent
IFT	Interfacial tension
IL	Ionic liquid
MD	Molecular dynamics
Ch	Choline
Cl	Chloride
U	Urea
EG	Ethylene glycol
M	Menthol
SA	Salicylic acid
HB	Hydrogen bonding
HBA	Hydrogen bonding acceptor
HBD	Hydrogen bonding donor
LJ	Lennard-Jones
VMD	Visual molecular dynamics

Data availability

All data in this article were produced using the publicly available GROMACS 2018.2 software.[65]

Conflicts of interest

There are no conflicts of interest to declare.

Acknowledgements

This work was supported by a research grant (DST/NSM/R&D_HPC_Applications/2021/13) from the National Supercomputing Mission (NSM), Government of India. We also extend our gratitude to the Department of Chemical and Biochemical Engineering at IIT Patna for providing the computing resources necessary for this study.

References

1 S. Thomas, Enhanced oil recovery-an overview, *Oil Gas Sci. Technol.*, 2008, **63**(1), 9–19.
2 A. Z. Abidin, T. Puspasari and W. A. Nugroho, Polymers for Enhanced Oil Recovery Technology, *Procedia Chem.*, 2012, **4**, 11–16.
3 S. Q. Tunio, A. H. Tunio, N. A. Ghirano and Z. M. El Adawy, Technology, Comparison of different enhanced oil recovery techniques for better oil productivity, *J. Int. J. Appl. Sci.*, 2011, **1**(5), 143–153.
4 A. Samanta, A. Bera, K. Ojha, A. Mandal and P. Technology, Comparative studies on enhanced oil recovery by alkali–surfactant and polymer flooding, *J. Pet. Explor.*, 2012, **2**, 67–74.
5 Y. Ahmadi; M. Mohammadi and M. Sedighi, Introduction to chemical enhanced oil recovery, *Chemical Methods*, Elsevier, 2022, pp. 1–32.
6 M. Sagir; M. Mushtaq; M. S. Tahir; M. B. Tahir and A. R. Shaik, *Challenges of Chemical EOR. In Surfactants for Enhanced Oil Recovery Applications*, ed. M. Sagir, M. Mushtaq, M. S. Tahir, M. B. Tahir and A. R. Shaik,

Springer International Publishing, Cham, 2020, pp. 117–129.
7 M. Ahmadi and Z. Chen, Challenges and future of chemical assisted heavy oil recovery processes, *Adv. Colloid Interface Sci.*, 2020, **275**, 102081.
8 A. Gbadamosi, S. Patil, M. S. Kamal, A. A. Adewunmi, A. S. Yusuff, A. Agi and J. Oseh, Application of Polymers for Chemical Enhanced Oil Recovery: A Review, *Polymers*, 2022, **14**(7), 1433.
9 B. N. Tackie-Otoo, M. A. Ayoub Mohammed, N. Yekeen and B. M. Negash, Alternative chemical agents for alkalis, surfactants and polymers for enhanced oil recovery: Research trend and prospects, *J. Pet. Sci. Eng.*, 2020, **187**, 106828.
10 A. O. Gbadamosi, R. Junin, M. A. Manan, A. Agi and A. S. Yusuff, An overview of chemical enhanced oil recovery: recent advances and prospects, *J. Int. Nano Lett.*, 2019, **9**, 171–202.
11 A. Sanati, S. Rahmani, A. Nikoo, M. Malayeri, O. Busse and J. Weigand, Comparative study of an acidic deep eutectic solvent and an ionic liquid as chemical agents for enhanced oil recovery, *J. Mol. Liq.*, 2021, **329**, 115527.
12 A. Bera, J. Agarwal, M. Shah, S. Shah and R. K. Vij, Recent advances in ionic liquids as alternative to surfactants/chemicals for application in upstream oil industry, *J. Ind. Eng. Chem.*, 2020, **82**, 17–30.
13 X. Wang, C. Dai, M. Zhao, X. Wang, X. Guo, P. Liu and Y. Qu, A novel property enhancer of clean fracturing fluids: Deep eutectic solvents, *J. Mol. Liq.*, 2022, **366**, 120153.
14 L. Yi, J. Feng, W. Li and Z. Luo, High-Performance Separation of Phenolic Compounds from Coal-Based Liquid Oil by Deep Eutectic Solvents, *ACS Sustainable Chem. Eng.*, 2019, **7**(8), 7777–7783.
15 J. Wang, W. Jing, H. Tian, M. Liu, H. Yan, W. Bi and D. D. Y. Chen, Investigation of Deep Eutectic Solvent-Based Microwave-Assisted Extraction and Efficient Recovery of Natural Products, *ACS Sustainable Chem. Eng.*, 2020, **8**(32), 12080–12088.
16 C. Fang, Y. Yang, S. Sun and R. Qiao, Low salinity effect on the recovery of oil trapped by nanopores: A molecular dynamics study, *Fuel*, 2020, **261**, 116443.
17 Y. Chen, Q. Xie and V. J. Niasar, Insights into the nanostructure of oil-brine-kaolinite interfaces: Molecular dynamics and implications for enhanced oil recovery, *Appl. Clay Sci.*, 2021, **211**, 106203.
18 C. Li, Y. Li and H. Pu, Molecular simulation study of interfacial tension reduction and oil detachment in nanochannels by Surface-modified silica nanoparticles, *Fuel*, 2021, **292**, 120318.
19 L. Fu, F. Gu, K. Liao, X. Wen, W. Huang, X. Li, Z. Ren and L. Xie, Engineering, Application of molecular simulation in tertiary oil recovery: A systematic review, *J. Pet. Sci.*, 2022, **212**, 110196.
20 M. Ahmadi and Z. Chen, Insight into the interfacial behavior of surfactants and asphaltenes: molecular dynamics simulation study, *Fuels*, 2020, **34**(11), 13536–13551.
21 D. Rodríguez-Llorente, A. Bengoa, G. Pascual-Muñoz, P. Navarro, V. I. Águeda, J. A. Delgado, S. Álvarez-Torrellas, J. García and M. Larriba, Sustainable Recovery of Volatile Fatty Acids from Aqueous Solutions Using Terpenoids and Eutectic Solvents, *ACS Sustainable Chem. Eng.*, 2019, **7**(19), 16786–16794.
22 T. Ahsani, Y. Tamsilian and A. Rezaei, Molecular dynamic simulation and experimental study of wettability alteration by hydrolyzed polyacrylamide for enhanced oil recovery: A new finding for polymer flooding process, *J. Pet. Sci. Eng.*, 2021, **196**, 108029.
23 A. F. Firooz, A. Hashemi, G. Zargar and Y. Tamsilian, Molecular dynamics modeling and simulation of silicon dioxide-low salinity water nanofluid for enhanced oil recovery, *J. Mol. Liq.*, 2021, **339**, 116834.
24 X. Dong; H. Liu and Z. Chen, Molecular dynamic simulation for hybrid enhanced oil recovery processes, *Developments in Petroleum Science*, Elsevier, 2021, vol. 73, pp. 207–228.
25 X. Yu, J. Li, Z. Chen, K. Wu, L. Zhang, G. Hui and M. Yang, Molecular dynamics computations of brine-CO_2/CH_4-shale contact angles: Implications for CO2 sequestration and enhanced gas recovery, *Fuel*, 2020, **280**, 118590.
26 D. Alfarge; M. Wei and B. Bai, Other enhanced oil recovery methods for unconventional reservoirs, in *Developments in Petroleum Science*, ed. D. Alfarge, M. Wei, B. Bai, B. Bai and Z. Chen, Elsevier, 2020, vol. 67, pp. 185–199.
27 C. Drummond and J. Israelachvili, Engineering, Surface forces and wettability, *J. Pet. Sci.*, 2002, **33**(1–3), 123–133.
28 S. Ma, X. Zhang, N. Morrow and X. Zhou, Characterization of wettability from spontaneous imbibition measurements, *J. Can. Pet. Technol.*, 1999, **38**, 13.
29 S. Stalheim, T. Eidesmo and H. Rueslåtten, Influence of wettability on water saturation modelling, *J. Pet. Sci. Eng.*, 1999, **24**(2–4), 243–253.
30 L. Coriand, N. Felde, N. Felde and A. Duparré, Wettability Behavior of Oleophilic and Oleophobic Nanorough Surfaces in Air or Immersed in Water. In Advances in Contact Angle, *Wettability Adhes.*, 2018, 167–178.
31 F. Ding and M. Gao, Pore wettability for enhanced oil recovery, contaminant adsorption and oil/water separation: A review, *J Adv. Colloid*, 2021, **289**, 102377.
32 K. Jarrahian, O. Seiedi, M. Sheykhan, M. V. Sefti and S. Ayatollahi, Wettability alteration of carbonate rocks by surfactants: A mechanistic study, *Colloids Surf., A*, 2012, **410**, 1–10.
33 Y. Yao, M. Wei and W. Kang, A review of wettability alteration using surfactants in carbonate reservoirs, *Adv. Colloid Interface Sci.*, 2021, **294**, 102477.
34 A. K. Manshad, M. Rezaei, S. Moradi, I. Nowrouzi and A. H. Mohammadi, Wettability alteration and interfacial tension (IFT) reduction in enhanced oil recovery (EOR) process by ionic liquid flooding, *J. Mol. Liq.*, 2017, **248**, 153–162.
35 S. Bhattacharjee, D. Chakraborty and S. Khan, Wetting behavior of aqueous 1-alkyl-3-methylimidazolium tetrafluoroborate {[Cn MIM][BF4](n = 2, 4, 6)} on graphite surface, *Chem. Eng. Sci.*, 2021, **229**, 116078.

36 A. Bera, Applications of ionic liquids as green solvents in enhanced oil recovery, in *Green Sustainable Process for Chemical and Environmental Engineering and Science*, ed. D. Inamuddin and T. Altalhi, Elsevier, 2023, pp. 125–144.
37 A. Bera, Applications of ionic liquids as green solvents in enhanced oil recovery, in *Green Sustainable Process for Chemical and Environmental Engineering and Science*, Elsevier, 2023, pp. 125–144.
38 P. Pillai, A. Kumar and A. Mandal, Mechanistic studies of enhanced oil recovery by imidazolium-based ionic liquids as novel surfactants, *J. Ind. Eng. Chem.*, 2018, **63**, 262–274.
39 S. K. Nandwani, N. I. Malek, M. Chakraborty and S. J. E. Gupta, Potential of a novel surfactant slug in recovering additional oil from highly saline calcite cores during the EOR process: synergistic blend of surface active ionic liquid and nonionic surfactant, *Fuels*, 2018, **33**(1), 541–550.
40 A. Bera and H. Belhaj, Ionic liquids as alternatives of surfactants in enhanced oil recovery—A state-of-the-art review, *J. Mol. Liq.*, 2016, **224**, 177–188.
41 A. R. Van Buuren, S. J. Marrink and H. J. Berendsen, A molecular dynamics study of the decane/water interface, *J. Phys. Chem. A*, 1993, **97**(36), 9206–9212.
42 M. Kunieda, *Molecular Dynamics Study of Oil–Water Interfacial Equilibrium in Petroleum Engineering*, 2012.
43 M. Kunieda, Y. Liang, Y. Fukunaka, T. Matsuoka, K. Takamura, N. Loahardjo, W. Winoto and N. R. Morrow, Spreading of multi-component oils on water, *Fuels*, 2012, **26**(5), 2736–2741.
44 J. Zhao, G. Yao, S. B. Ramisetti, R. B. Hammond and D. Wen, Molecular dynamics simulation of the salinity effect on the n-decane/water/vapor interfacial equilibrium, *Energy Fuels*, 2018, **32**(11), 11080–11092.
45 S. Sakthivel and M. Elsayed, Enhanced oil recovery by spontaneous imbibition of imidazolium based ionic liquids on the carbonate reservoir, *J. Mol. Liq.*, 2021, **340**, 117301.
46 H. Weingärtner, Understanding ionic liquids at the molecular level: facts, problems, and controversies, *Angew. Chem., Int. Ed.*, 2008, **47**(4), 654–670.
47 E. L. Smith, A. P. Abbott and K. S. Ryder, Deep eutectic solvents (DESs) and their applications, *Chem. Rev.*, 2014, **114**(21), 11060–11082.
48 D. J. G. P. van Osch, C. H. J. T. Dietz, J. van Spronsen, M. C. Kroon, F. Gallucci, M. van Sint Annaland and R. Tuinier, A Search for Natural Hydrophobic Deep Eutectic Solvents Based on Natural Components, *ACS Sustainable Chem. Eng.*, 2019, **7**(3), 2933–2942.
49 M. Gilmore, É. N. McCourt, F. Connolly, P. Nockemann, M. Swadźba-Kwaśny and J. D. Holbrey, Hydrophobic Deep Eutectic Solvents Incorporating Trioctylphosphine Oxide: Advanced Liquid Extractants, *ACS Sustainable Chem. Eng.*, 2018, **6**(12), 17323–17332.
50 M. Atilhan, L. T. Costa and S. Aparicio, Elucidating the Properties of Graphene–Deep Eutectic Solvents Interface, *Langmuir*, 2017, **33**(21), 5154–5165.
51 M. Atilhan and S. Aparicio, Engineering, Molecular dynamics study on the use of Deep Eutectic Solvents for Enhanced Oil Recovery, *J. Pet. Sci.*, 2022, **209**, 109953.
52 A. Hebbar, D. Debraj, S. Acharya, S. K. Puttapati, A. K. Vatti and P. Dey, Deep eutectic solvents interaction with asphaltenes: A combined experimental and molecular dynamics study, *J. Mol. Liq.*, 2023, **387**, 122627.
53 M. K. Hadj-Kali, K. E. Al-khidir, I. Wazeer, L. El-blidi, S. Mulyono and I. M. AlNashef, Application of deep eutectic solvents and their individual constituents as surfactants for enhanced oil recovery, *Colloids Surf., A*, 2015, **487**, 221–231.
54 A. El-hoshoudy, F. Soliman, E. Mansour, T. Zaki and S. Desouky, Experimental and theoretical investigation of quaternary ammonium-based deep eutectic solvent for secondary water flooding, *J. Mol. Liq.*, 2019, **294**, 111621.
55 D. S. Raut, V. A. Joshi, S. Khan and D. Kundu, A-Priori screening of deep eutectic solvent for enhanced oil recovery application using COSMO-RS framework, *J. Mol. Liq.*, 2023, **377**, 121482.
56 L. Martínez, R. Andrade, E. G. Birgin and J. M. Martínez, PACKMOL: a package for building initial configurations for molecular dynamics simulations, *J. Comput. Chem.*, 2009, **30**(13), 2157–2164.
57 H. Krienke and D. Opalka, Hydration of molecular ions: A molecular dynamics study with a SPC/E water model, *J. Phys. Chem. C*, 2007, **111**(43), 15935–15941.
58 P. Mark and L. Nilsson, Structure and dynamics of the TIP3P, SPC, and SPC/E water models at 298 K, *J. Phys. Chem. A*, 2001, **105**(43), 9954–9960.
59 B. Qiao and W. Jiang, All-Atom Molecular Dynamics Study of Water–Dodecane Interface in the Presence of Octanol, *J. Phys. Chem. C*, 2018, **122**(1), 687–693.
60 Q. Liu, X. Zhang, Q. Zhang, T. Wang and B. Jiang, Molecular dynamics simulations of dodecane detachment from hydrophobic SiO2 surfaces in CTAB solutions, *Colloids Surf., A*, 2022, **653**, 130020.
61 R. Mahfud, Molecular Dynamics Computational Study of Sustainable Green Surfactant for Application in Chemical Enhanced Oil Recovery, *ACS Omega*, 2024, **9**(25), 27177–27191.
62 E. P. Maiki, R. Sun, S. Ren and A. M. AlRassas, Experimental and Molecular Dynamics Simulation to Investigate Oil Adsorption and Detachment from Sandstone/Quartz Surface by Low-Salinity Surfactant Brines, *ACS Omega*, 2024, **9**(18), 20277–20292.
63 W. Humphrey, A. Dalke and K. Schulten, VMD: visual molecular dynamics, *J. Mol. Graphics*, 1996, **14**(1), 33–38.
64 S. Xiao, S. A. Edwards and F. Gräter, A New Transferable Forcefield for Simulating the Mechanics of $CaCO_3$ Crystals, *J. Phys. Chem. C*, 2011, **115**(41), 20067–20075.
65 M. J. Abraham, T. Murtola, R. Schulz, S. Páll, J. C. Smith, B. Hess and E. Lindahl, GROMACS: High performance molecular simulations through multi-level parallelism from laptops to supercomputers, *SoftwareX*, 2015, **1–2**, 19–25.
66 B. Doherty and O. Acevedo, OPLS force field for choline chloride-based deep eutectic solvents, *J. Phys. Chem. B*, 2018, **122**(43), 9982–9993.

67 W. L. Jorgensen and J. Tirado-Rives, Potential energy functions for atomic-level simulations of water and organic and biomolecular systems, *Proc. Natl. Acad. Sci. U. S. A.*, 2005, **102**(19), 6665–6670.
68 L. S. Dodda, J. Z. Vilseck, J. Tirado-Rives and W. L. Jorgensen, 1.14*CM1A-LBCC: Localized Bond-Charge Corrected CM1A Charges for Condensed-Phase Simulations, *J. Phys. Chem. B*, 2017, **121**(15), 3864–3870.
69 L. S. Dodda, I. Cabeza de Vaca, J. Tirado-Rives and W. L. Jorgensen, LigParGen web server: an automatic OPLS-AA parameter generator for organic ligands, *Nucleic Acids Res.*, 2017, **45**(W1), W331–W336.
70 E. R. Cruz-Chu, A. Aksimentiev and K. Schulten, Water−Silica Force Field for Simulating Nanodevices, *J. Phys. Chem. B*, 2006, **110**(43), 21497–21508.
71 H. A. Lorentz, Ueber die Anwendung des Satzes vom Virial in der kinetischen Theorie der Gase, *Ann. Phys.*, 1881, **248**(1), 127–136.
72 T. Darden, D. York and L. Pedersen, Particle mesh Ewald: An N log (N) method for Ewald sums in large systems, *J. Chem. Phys.*, 1993, **98**(12), 10089–10092.
73 A. Gutiérrez, M. Atilhan and S. Aparicio, Molecular dynamics study on water confinement in deep eutectic solvents, *J. Mol. Liq.*, 2021, **339**, 116758.
74 A. Korotkevich, D. S. Firaha, A. A. H. Padua and B. Kirchner, Ab initio molecular dynamics simulations of SO2 solvation in choline chloride/glycerol deep eutectic solvent, *Fluid Phase Equilib.*, 2017, **448**, 59–68.
75 Y. Li, Y. Li, H. Li, X. Fan, H. Yan, M. Cai, X. Xu and M. Zhu, Insights into the tribological behavior of choline chloride—urea and choline chloride—thiourea deep eutectic solvents, *Friction*, 2023, **11**(1), 76–92.
76 L. Wang, Y. Cui, J. Li, Z. Song, H. Cheng and Z. Qi, Toward high-performance associative extraction by forming deep eutectic solvent: A component pairing and mechanism study, *Chem. Eng. Sci.*, 2023, **272**, 118602.
77 A. Luzar and D. Chandler, Hydrogen-bond kinetics in liquid water, *Nature*, 1996, **379**(6560), 55–57.
78 A. Kumar, S. Medha, D. Chakraborty, D. Kundu and S. Khan, Wetting and interfacial behavior of aqueous Deep eutectic solvents on Graphite, silica and calcite surfaces: Molecular dynamics study, *Chem. Eng. Sci.*, 2024, 120231.
79 J. G. Kirkwood and F. P. Buff, The Statistical Mechanical Theory of Solutions, *J. Chem. Phys.*, 2004, **19**(6), 774–777.
80 E. Rilo, J. Pico, S. García-Garabal, L. M. Varela and O. Cabeza, Density and surface tension in binary mixtures of CnMIM-BF4 ionic liquids with water and ethanol, *Fluid Phase Equilib.*, 2009, **285**(1), 83–89.
81 Z. N. Z. Martin, I. S. Martinez and R. B. Nellas, Surface tension data of n-propane, n-octane and n-dodecane from nucleation simulations, *Tellus B*, 2018, **70**(1), 1–5.
82 T. Bui, H. Frampton, S. Huang, I. R. Collins, A. Striolo and A. Michaelides, Water/oil interfacial tension reduction – an interfacial entropy driven process, *Phys. Chem. Chem. Phys.*, 2021, **23**(44), 25075–25085.
83 R. Wardhani, D. R. Husain and F. Gani, Reduction of surface tension of petroleum using hydrocarbon degrading bacterial activity, *ASM Sci.*, 2022, **17**, 1–6.
84 C. Jian, M. R. Poopari, Q. Liu, N. Zerpa, H. Zeng and T. Tang, Reduction of Water/Oil Interfacial Tension by Model Asphaltenes: The Governing Role of Surface Concentration, *J. Phys. Chem. B*, 2016, **120**(25), 5646–5654.
85 A. Mohsenzadeh, Y. Al-Wahaibi, A. Jibril, R. Al-Hajri and S. Shuwa, The novel use of deep eutectic solvents for enhancing heavy oil recovery, *J. Pet. Sci. Eng.*, 2015, **130**, 6–15.